ARTICLES

Rovibrational Relaxation of Methane in CH_4-N_2 Mixtures: Time-Resolved IR−IR Double-Resonance Measurements at 193 K and Kinetic Modeling

Corinne Boursier,* Joseph Ménard, Lucien Doyennette, and Françoise Menard-Bourcin

Laboratoire de Physique Moléculaire et Applications, CNRS, Université Pierre et Marie Curie, Tour 13−Bte 76, 4 place Jussieu, 75252 Paris Cedex 05, France

Received: January 31, 2003; In Final Form: April 25, 2003

Measurements have been conducted in methane and methane−nitrogen mixtures at 193 K by means of a time-resolved IR−IR double-resonance technique. Methane molecules were excited into selected rotational levels of the $2\nu_3(F_2)$ state near 6000 cm^{-1}. By probing with a tunable laser diode the $3\nu_3-2\nu_3(F_2)$ transitions in which the lower level is the laser-excited level, rotational depopulation rates were measured. They were found to be equal to (28.3 ± 3.0) $\mu s^{-1}Torr^{-1}$ and (21.5 ± 3.0) $\mu s^{-1}Torr^{-1}$, respectively, for self- and CH_4-N_2 collisions. By probing other stretching transitions such as $2\nu_3(F_2)-\nu_3$, $(\nu_3 + 2\nu_4)-2\nu_4$, and $(\nu_3 + \nu_4)-\nu_4$ transitions, various vibrational relaxation processes were investigated. A numerical kinetic model, taking into account many collisional processes connecting energy levels up to 6000 cm^{-1}, has been developed to describe vibrational relaxation. This model allowed us to reproduce observed double-resonance signals and to determine rate coefficients for various relaxation processes. Furthermore, the good agreement between computed and observed signals is encouraging for using this model to predict the time evolution of populations of methane energy levels especially for pressure or mixing ratio values that cannot be realized in our experiments.

I. Introduction

The present work is the continuation of previous investigations[1,2] concerning rovibrational energy transfer in methane and methane−nitrogen mixtures after laser excitation of CH_4 molecules into the $2\nu_3(F_2)$ manifold. In these previous studies, on the basis of the time-resolved double-resonance technique, rotational depopulation rates for $2\nu_3(F_2)$ levels were measured at room temperature for CH_4-CH_4 as well as CH_4-N_2 collisions, and the time evolution of several tetradecad, pentad, or dyad states could be investigated, providing information on relevant relaxation pathways. The first purpose of the present work is to carry out similar measurements at lower temperature, which is more relevant for applications to the terrestrial atmosphere or to the atmosphere of Titan.[3,4] The second purpose is to develop a numerical model based on a kinetic scheme able to retrieve from the double-resonance (DR) signals the rate coefficients of the various collisional processes involved.

After briefly recalling in section II the experimental setup and the vibrational energy-level diagram of CH_4, the experimental results obtained on the rotational relaxation are presented and discussed in section III. Section IV deals with the vibrational relaxation: the corresponding experimental results are first shown; then the kinetic model with the various processes involved in the vibrational relaxation is described; and finally, simulations of DR signals using the kinetic model are presented and the values of the rate coefficients corresponding to the different processes are given at 193 K and at room temperature.

II. Experimental Section

The experimental conditions are very similar to those described in previous papers[1,2] except for the double-resonance cell. Methane molecules are excited into selected rotational levels of the $2\nu_3(F_2)$ state by the single-mode output beam of an OPO laser pumped by a single-mode pulsed Nd:YAG laser (Continuum). The time evolution of rovibrational populations consecutive to laser excitation is monitored with the low-power beam of a cw single-mode lead-salt diode laser (Laser Photonics). The emitting range of this diode allowed us to probe various transitions of $\Delta v_3 = \pm 1$ harmonic or combination bands between 2939 and 2983 cm^{-1}. A simplified diagram of the CH_4 vibrational energy levels up to about 9000 cm^{-1} is given in Figure 1. Let us recall that all of these levels are gathered in polyads of interacting states. The different kinds of transitions probed in our experiments are dyad−octad, pentad−tetradecad, and tetradecad−P_6 transitions as shown in this Figure.

The double-resonance cell through which the pump and probe beams propagate has been modified to operate at temperatures down to 190 K (see Figure 2).

The coolable sample cell is a 68-cm-long Pyrex glass tube with an internal diameter of 3.8 cm, sealed by ZnS windows and fitted by a Teflon valve. The cell is enclosed by two jackets over almost the entire length. The outer vacuum jacket serves as thermal insulation whereas chilled ethanol circulates in the internal one. A mechanical refrigerator (Maton) is used to chill the ethanol and circulate it through insulated transfer tubes to and from the cell at a regulated temperature measured by a Pt-100 probe at the refrigerator outlet. The cell temperature is controlled by a chromel−alumel thermocouple placed at the coolant outlet. The difference between temperatures measured by the Pt probe and the thermocouple did not exceed 1 K. During the experiments, the temperature fluctuations did not exceed ±0.5 K. A gentle nitrogen flow was blown on the cell windows to prevent moisture deposition.

* Corresponding author. E-mail: boursier@ccr.jussieu.fr. Fax: 33 (0)1 44 27 70 33.

10.1021/jp034265m CCC: $25.00
Published on Web 06/12/2003

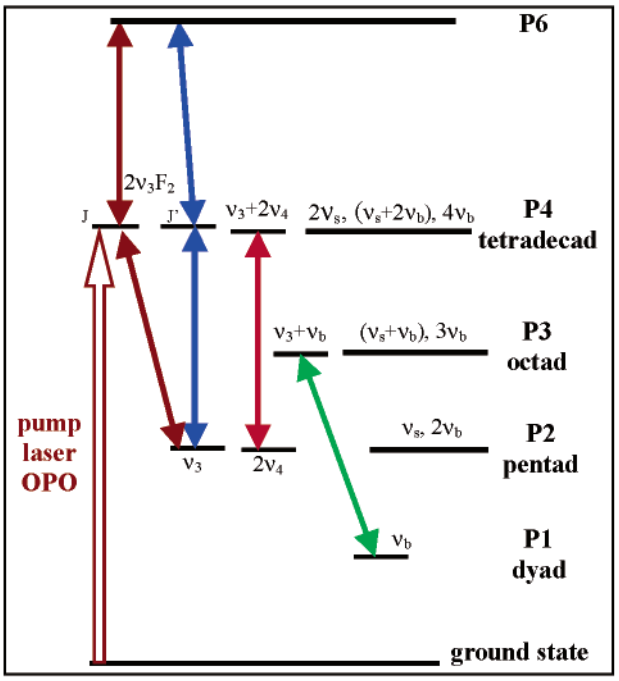

Figure 1. Simplified diagram of the CH_4 vibrational energy levels up to the P6 polyad with laser excitation and the main types of probed transitions. ν_b corresponds to bending mode ν_2 or ν_4, and ν_s, to stretching mode ν_1 or ν_3.

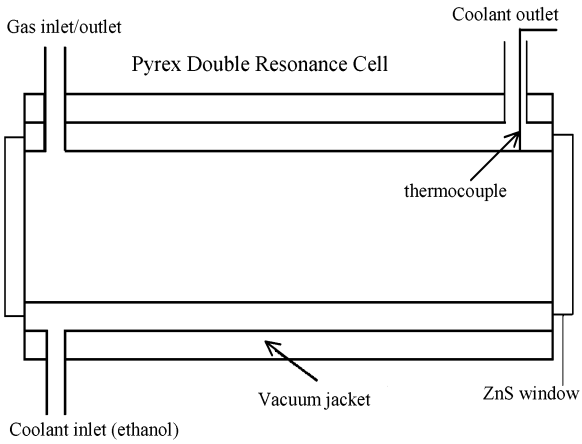

Figure 2. Configuration of the coolable cell.

Our measurements have been performed in neat methane and in CH_4-N_2 mixtures at 193 K for different gas pressures and by varying the methane molar fraction in the gas mixtures.

III. Rotational Relaxation

A. Experimental Results. The most direct way to measure total rotational depopulation rates after excitation into the $2\nu_3(F_2)$ state by an IR−IR DR technique is to probe a transition in which the lower level is the laser-excited level. Despite the lack of spectroscopic data on the transitions between the tetradecad and the P6 polyad whose energy is about 9000 cm^{-1}, we were able to find some transitions[1] between $2\nu_3(F_2)$ and a state of the P6 polyad (probably $3\nu_3$) in the emitting range of the laser diode. For many of these P6−$2\nu_3(F_2)$ transitions, we could assign without ambiguity the rotational quantum number J and the symmetry of the lower level. Indeed, it is now well established[5−7] that in the gas phase the nuclear spin state is conserved during collisional processes, so we have carried out, with the probes at our disposal, measurements in methane and in methane−nitrogen mixtures with methane molar fractions

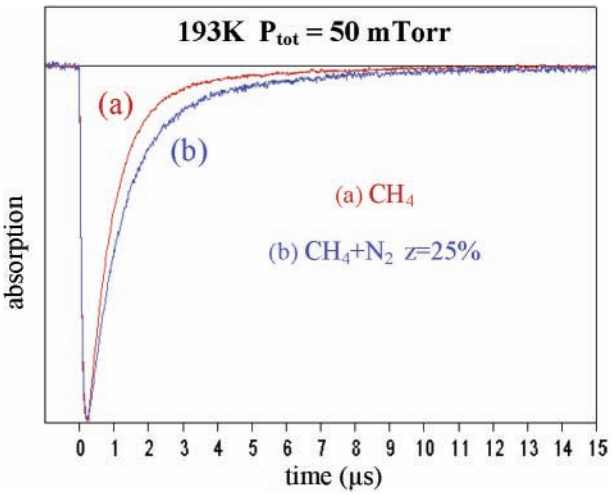

Figure 3. DR signal observed after excitation via the P_3 line of the $2\nu_3(F_2) \leftarrow 0$ band by probing the laser-excited level via a P6−$2\nu_3(F_2)$ transition. The depletion of the $J = 2$ rotational level that corresponds to the rising part of the signal is only slightly slowed in the mixture.

from 5 to 25%. Two DR signals obtained by exciting the molecules into the $2\nu_3(F_2)$ $J = 2$, A_1, 29 state[8] via the P_3 line of the $2\nu_3(F_2) \leftarrow 0$ band and probing the laser-excited level via a transition at 2944.53 cm^{-1} are shown in Figure 3. They exhibit first a very intense and quasi-instantaneous initial absorption (in the limit of our detection electronics). The rise following this initial decay is due to the depletion of the laser-excited rotational state. For both signals, the total gas pressure in the sample cell was 50 mTorr; one signal (a) was obtained in pure methane, and the other one (b), in a CH_4-N_2 mixture with a methane molar fraction z equal to 25%. This Figure is illustrative of the efficiency of CH_4-N_2 collisions relative to that of CH_4-CH_4 collisions: indeed, the rising part of the signal is only slightly slowed in the mixture. This rising part is well fitted by a sum of two exponential functions of time, and the pressure-dependent rotational relaxation rate is retrieved from the fastest exponential function.

Another way to have access to rotational de-excitation is to probe a $2\nu_3(F_2)-\nu_3$ transition in which the laser-excited level is now the upper level of the probed transition. Such a signal is given in Figure 4. In this case, the depletion of the laser-excited level corresponds to the decaying part of the amplification of the probe beam, and the rotational relaxation rate is retrieved from the DR signal similarly to the previous case of $2\nu_3(F_2)-$P6 transitions.

After a series of measurements performed either by probing P6−$2\nu_3(F_2)$ or $2\nu_3(F_2)-\nu_3$ transitions in various mixtures and pressure conditions with time × pressure scales lower than 1 μs × Torr, the rotational rate constant (i.e., the rotational rate divided by the total pressure) was found to vary linearly with the molar fraction z. A linear regression yields (28.3 ± 3.0) μs^{-1} $Torr^{-1}$ and (21.5 ± 3.0) μs^{-1} $Torr^{-1}$ for rotational relaxation rates upon CH_4-CH_4 and CH_4-N_2 collisions, respectively. No significant difference was observed between the rotational depopulation rate constants of the $2\nu_3(F_2)$ rotational levels that we could investigate, namely, A symmetry levels with J ranging from 1 to 4. Let us recall that the corresponding values that we have obtained[2] at 296 K were smaller (i.e., (20.8 ± 2.5) μs^{-1} $Torr^{-1}$ and (13.0 ± 1.5) μs^{-1} $Torr^{-1}$, respectively).

B. Discussion. To assess the consistency of our results on rotational relaxation with existing results, one has to refer to line-broadening studies because, to our knowledge, no rotational

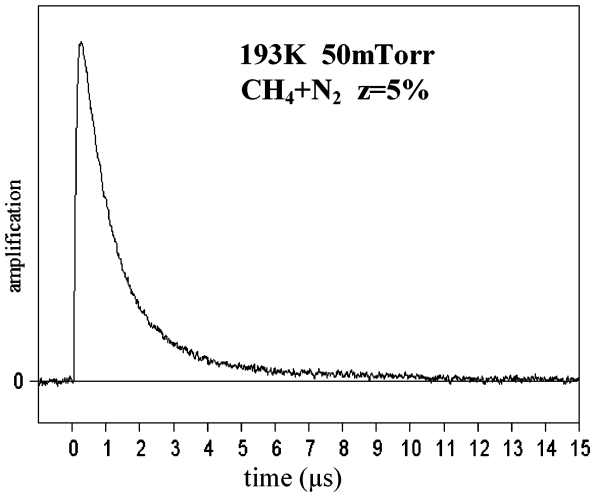

Figure 4. DR signal observed after excitation into the $2\nu_3(F_2)$ $J = 1$, A_2, 18 level via the R_0 line of the $2\nu_3(F_2) \leftarrow 0$ band by probing the laser-excited level via the P_2 line of $2\nu_3(F_2)-\nu_3$ at 2963.99 cm^{-1}. The decreasing part of the signal corresponds to the depletion of the $J = 1$ rotational state.

relaxation measurements were performed in methane at low temperature except for supersonic expansion measurements[9] in CH_4-Ar mixtures. Assuming that the upper and lower levels of a given transition have the same total depopulation rate constant k, the broadening coefficient γ/P may be approximately related to k by the following equation: $(\gamma/P) = (k/2\pi c)$ where c is the velocity of light in vacuum. In many papers, dealing with self- or N_2-broadening,[10−13] broadening coefficients were found to be dependent on the rotational quantum number J and on the symmetry. From the paper by Smith et al.[13] on the temperature dependence of N_2- and air-broadening coefficients, one gets for the A species lines in our J range an N_2-broadening coefficient of (0.060 ± 0.003) cm^{-1} atm^{-1} at 296 K and a temperature exponent of 0.75 leading to a broadening coefficient of 0.083 ± 0.004 at 193 K. This gives, using the above equation, an equivalent rotational relaxation rate constant upon CH_4-N_2 collisions of (20.6 ± 1.0) μs^{-1} $Torr^{-1}$, which is close to our result of (21.5 ± 3.0) μs^{-1} $Torr^{-1}$. For self-collisions, the comparison is more difficult because no study has been devoted to the temperature dependence of the self-broadening coefficient. However, an estimation of the self-broadening coefficient at 193 K may be obtained by an interpolation between the results at room temperature and those at 77 K. At 296 K, the results of Pine[10] in the ν_3 band as well as the results of Boussin et al.[14] in the 5500−6180 cm^{-1} range led us to take (0.081 ± 0.003) cm^{-1} atm^{-1} for the self-broadening coefficient in our range of J values. At 77 K, from the studies of Singh et al.[15] or of Varanasi et al.,[16] the self-broadening coefficient ranges from 0.22 to 0.35 cm^{-1} atm^{-1}. Combining these values results in an estimated rotational relaxation rate constant corresponding to self-collisions between 27 and 32 μs^{-1} $Torr^{-1}$, which is again close to our result of (28.3 ± 3.0) μs^{-1} $Torr^{-1}$.

Finally, let us notice that for 1 Torr of any mixture the rotational relaxation is achieved within 250 ns. Then, the assumption of rotational equilibration should be valid when studying vibrational relaxation on time × pressure scales larger than those used in this section.

IV. Vibrational Relaxation

A. Experimental Results. By probing successively, in the same gas sample, transitions belonging to different bands, one gets an interesting overview of the relaxation pathways. For instance, Figure 5 presents on a same time scale four DR signals

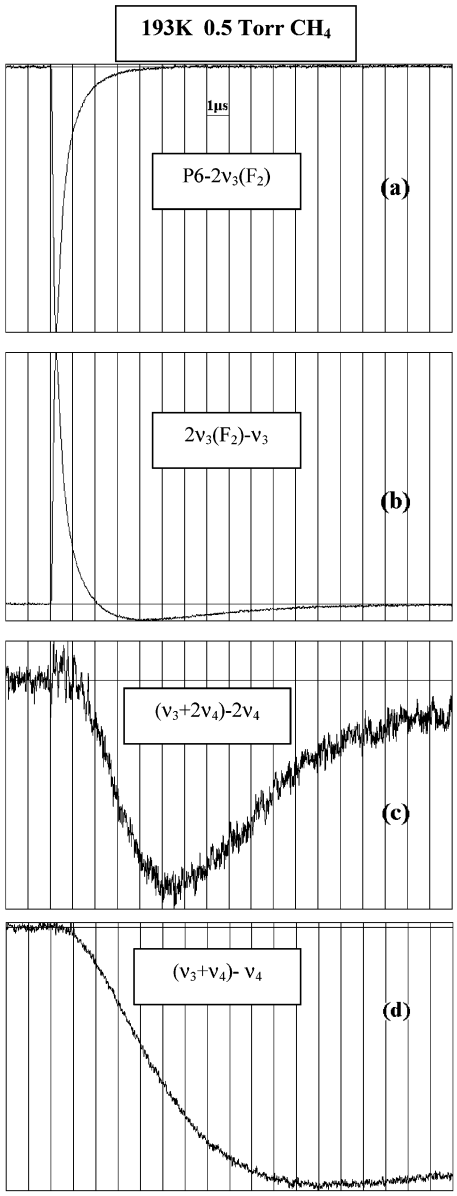

Figure 5. DR signals obtained at 193 K in pure CH_4 by exciting methane into the $2\nu_3(F_2)$ $J = 1$, A_2, 18 level and by probing four different transitions involving A-symmetry species: (a) the $P6-2\nu_3(F_2)$ transition at 2944.53 cm^{-1}, (b) the $2\nu_3(F_2)-\nu_3$ transition at 2944.69 cm^{-1}, (c) a $(\nu_3 + 2\nu_4)-2\nu_4$ transition, and (d) an octad−dyad transition. The time scale is the same for all signals: 1 μs/division.

obtained at 193 K in 0.5 Torr of methane after excitation into the $2\nu_3(F_2)$ $J = 1$, A_2, 18 level via the R_0 line of the $2\nu_3(F_2) \leftarrow 0$ band. The four probed transitions also involve A symmetry species. In signal a, the probed transition is the $P6-2\nu_3(F_2)$ $J = 2$, A_1, 29 transition at 2944.53 cm^{-1}. The next two signals are obtained by probing tetradecad−pentad transitions: the $2\nu_3(F_2)$ $J = 3$, A_1, $32-\nu_3$ $J = 4$, A_2, 5 transition (signal b) or a $(\nu_3 + 2\nu_4)-2\nu_4$ transition (signal c) whereas the last one corresponds to an octad−dyad transition.

Although signal a of Figure 5 looks similar to the signals of Figure 3 and is obtained with the same probe, it does not illustrate the same relaxation processes because in Figure 5 the time × pressure scale is 10 times larger than that used in Figure 3 and the probed level is not the laser-excited level. The fast initial rise in absorption of signal a is due to rotational-energy transfer from the laser-excited level $J = 1$ to the probed level $J = 2$; then the absorption of the probed beam returns to its

equilibrium value within 6 μs, showing that the probed level returns to its equilibrium population by energy transfer toward other tetradecad states or lower polyads. For signal b, the $2\nu_3(F_2)$ $J = 3$ tetradecad level is now the upper level of the probed transition. Hence, the beginning of signal b is almost symmetric to signal a, presenting a fast initial amplification as the upper level of the transition is populated upon rotational-energy transfer from the laser-excited level followed by a decrease as the upper level is depleted. Moreover, the absorbed part of signal b reveals an increase in the population of the ν_3 $J = 4$ lower level of the transition. The depletion of $2\nu_3(F_2)$ is due both to several intermode energy transfer processes that redistribute vibrational energy among the tetradecad and to vibration−vibration energy transfer to lower polyads. This is clearly seen by comparing signals a and b, which shows that the ν_3 pentad level becomes more populated than the $2\nu_3(F_2)$ tetradecad level before the complete depletion of this tetradecad level. The intermode energy transfer from stretching to bending modes inside the tetradecad can be seen on signal c for which the upper level of the probed transition belongs to the $(\nu_3 + 2\nu_4)$ vibrational state. Indeed, during the first microsecond, signal c exhibits a slight amplification showing an increase in the population of the upper level of the probed transition. Next, signal c displays the absorption of the probe beam due to the filling of $2\nu_4$, the lower level of the probed transition, which is similar to what happens in signal b for the ν_3 state. In both signals, the absorption reaches a maximum near 5 μs corresponding to a maximum in the transient population of the lower level, ν_3 or $2\nu_4$. This means that bending and stretching states of the pentad have similar relaxation characteristics. Finally, signal d shows increasing absorption as ν_4, the lowest vibrational state, is filled through the successive energy transfer processes that spread out energy from the tetradecad to lower polyads. The population of ν_4 reaches a maximum around 12 μs and begins to decrease. The time × pressure scale used in Figure 5 is clearly not suitable to study the time evolution of dyad states, so for each kind of probe, measurements in methane and methane−nitrogen mixtures have been made with various methane molar fractions at the appropriate time × pressure scale to determine the contribution of methane−nitrogen collisions and to cover a large range of experimental conditions in order to test our kinetic model.

1. Tetradecad and Pentad States Probing. As described above, the depletion of the $2\nu_3(F_2)$ state is observed by probing P6$-2\nu_3(F_2)$ transitions in which the lower level is not the laser-excited level. Two DR signals obtained, either in 200 mTorr of pure methane or in 200 mTorr of methane mixed with 1.8 Torr of nitrogen, by probing the P6$-2\nu_3(F_2)$ $J = 2$, A_1, 29 transition at 2970.93 cm^{-1} after excitation into the $2\nu_3(F_2)$ $J = 4$, A_2, 43 level via Q_4 are presented in Figure 6.

Adding nitrogen to methane enhances the depletion of the $2\nu_3(F_2)$ probed level, showing that intermode transfer processes are also occurring upon CH_4-N_2 collisions as well as upon self-collisions and contribute significantly to the depletion of tetradecad states. This is confirmed by probing the $2\nu_3(F_2)$ $J = 1$, A_2, 18$-\nu_3$ $J = 2$, A_1, 4 transition in the same gas samples, as can be seen in Figure 7. The small absorption part of the DR signal for $CH_4 + N_2$ demonstrates again an increase in the population of ν_3 but to a lesser extent than in the case of pure methane.

The temperature dependence of such signals is illustrated in Figure 8 , showing two DR signals obtained by probing the same $2\nu_3(F_2)-\nu_3$ transition for the same pressure of methane at 193 K and at room temperature. For a given pressure, the depletion of the tetradecad is faster, and the population of ν_3 reaches a maximum earlier at 193 K than at 296 K.

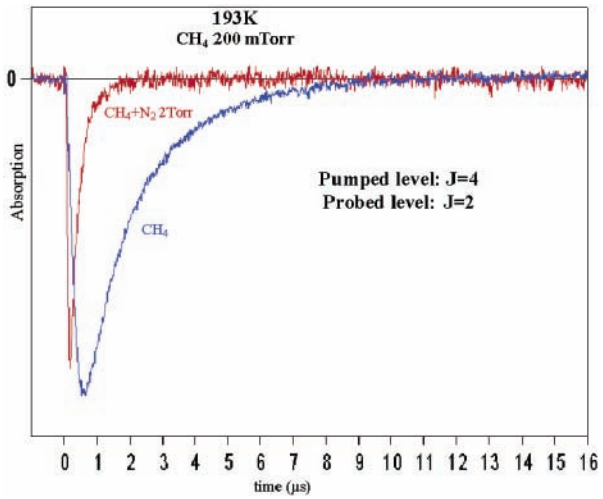

Figure 6. Effect of CH_4-N_2 collisions on the depletion of the $2\nu_3(F_2)$ vibrational state. It is observed by probing a P6$-2\nu_3(F_2)$ transition in which the lower level is not the laser-excited level. Both signals are obtained for the same methane pressure.

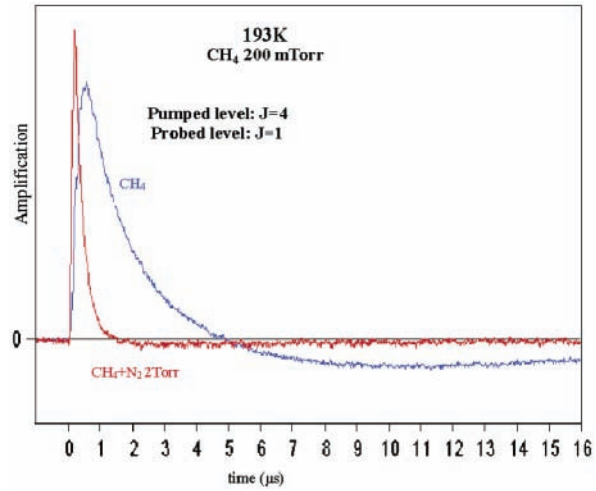

Figure 7. By probing the $(2\nu_3(F_2)$ $J = 1$, A_2, 18$)-(\nu_3$ $J = 2$, A1, 4) transition at 2963.99 cm^{-1} after excitation into the $(2\nu_3(F_2)$ $J = 4$, A_2, 43) level, filling of the ν_3 state as well as depletion of the $2\nu_3(F_2)$ state is observed.

It is worth noting that when looking at signals obtained with the same pressure at different temperatures one compares pressure-scaled rate constants such as in line-broadening studies, but when comparing signals obtained with the same number of molecules, one gets information on concentration-scaled rate constants that are related to the former by a factor proportional to the temperature. Indeed, for the same concentration, the depletion of the tetradecad appears slightly faster at room temperature than at 193 K.

2. Dyad States Probing. The dyad states, especially ν_4, are studied by probing octad−dyad transitions. In the example already given in Figure 5d, the probed transition involved the same symmetry species as for the excited level, and the DR signal gave the time evolution of ν_4 levels with A spin modification. The time evolution of ν_4 levels of a symmetry type different from that of the pumped level can also be investigated by probing octad−dyad transitions of the appropriate symmetry. Figure 9 allows a comparison of the behavior of a ν_4 A-symmetry level with that of a ν_4 F-symmetry level after laser excitation into a $2\nu_3(F_2)$ A-symmetry level.

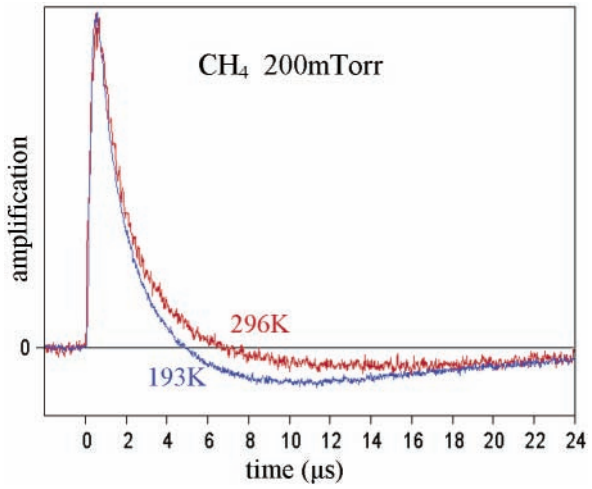

Figure 8. DR signals obtained by probing the same $2\nu_3(F_2)-\nu_3$ transition at 2963.99 cm^{-1} at the same methane pressure at 193 K and at room temperature.

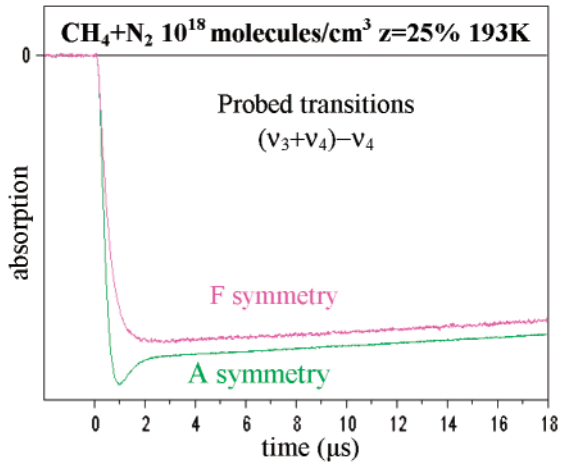

Figure 9. DR signals obtained in the same gas sample either an A-symmetry- or an F-symmetry-type octad−dyad transition after excitation on a tetradecad level of the A-symmetry species.

The two DR signals of Figure 9 are obtained at 193 K in a methane−nitrogen mixture at 20 Torr with molar fraction $z = 0.25$. The filling of the A-symmetry level is faster than that of the F-symmetry level, the population of the A-symmetry level reaching a maximum in about 1 μs. Then the A-symmetry population decreases while the population of the F-symmetry level is still increasing, reaching a maximum in about 3 μs. After that, both populations decrease slowly at the same speed, corresponding to vibration-to-translation/rotation (V−T/R) energy transfer (loss of a ν_4 quantum). These features were already observed at room temperature[2] and may be explained by the conservation of the spin modification in collisional processes and by cascading near-resonant vibration−vibration (V−V) energy transfer in the ν_4 mode that induces an increase in the population of the ν_4 state. Indeed, in the V−V cascading de-excitation scheme, one molecule excited in a tetradecad A-symmetry level gives one molecule in an octad A-symmetry level, and another molecule is promoted from the ground state to the dyad, keeping its spin modification (A, E, or F) and so on from the octad to the pentad and from the pentad to the dyad. Consequently, the filling of the ν_4 F-symmetry levels is due only to the promotion of molecules from the ground state whereas the filling of the ν_4 A-symmetry levels is due to the promotion from the ground state but also to de-excitation from the tetradecad A-symmetry levels. This implies a temporary excess in the population of the ν_4 A-symmetry levels with respect to the equilibrium distribution of the different spin modifications ($^5/_{16}$ in A, $^2/_{16}$ in E, and $^9/_{16}$ in F). This temporary excess disappears by vibrational swap between the dyad and the ground state. In the experimental conditions of Figure 9, the return to the equilibrium distribution of ν_4 levels between the three symmetry species is achieved within 4 μs, and then all of the levels return to Boltzmann equilibrium very slowly by V−T/R transfer processes.

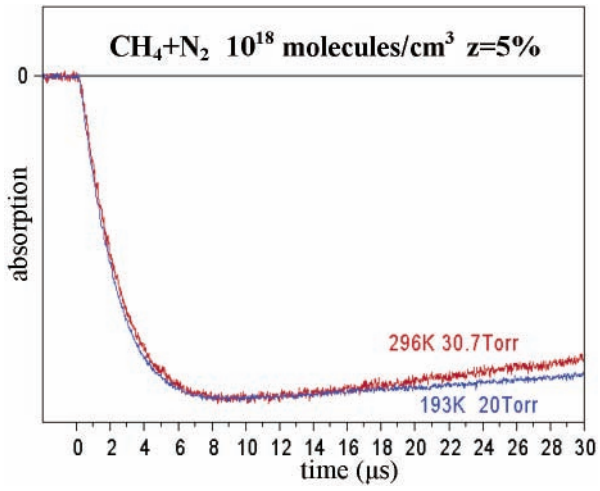

Figure 10. Effect of temperature on the filling of the dyad. Both DR signals are obtained by probing the same F-symmetry $(\nu_3 + \nu_4)-\nu_4$ transition in the same gas sample after excitation of the $2\nu_3(F_2)$ $J = 1$, A_2, 18 level.

By examining DR signals obtained in mixtures with methane molar fractions from 5 to 25%, the time to reach a population maximum either in ν_4 A-symmetry levels or in ν_4 F-symmetry levels was found to be independent of the nitrogen pressure. This implies that, in this range of z, the temporal evolution of the ν_4 states population depends essentially on V−V near-resonant processes occurring only upon self-collisions. Indeed, intermode processes should be very fast with respect to the processes of ν_4 quantum exchange, and V−T de-excitation very slow.

To examine the temperature dependence of these processes, a DR signal obtained at 193 K by probing an octad−dyad F-symmetry transition in a methane−nitrogen mixture, after excitation in a tetradecad A-symmetry level, is compared in Figure 10 to a signal obtained at 296 K with the same pump/probe combination in the same gas sample, the number of molecules in the sample cell being unchanged. The comparison demonstrates that cascading V−V processes filling the ν_4 levels are faster at 193 K than at 296 K. On the contrary, V−T/R processes that deplete the dyad are slower at 193 K than at 296 K.

B. Kinetic Model. As methane molecules are excited into rotational levels of the tetradecad, the number of rovibrational levels implied in the relaxation process is huge. However, as described in section III, the average rotational de-excitation rate is fast enough, even for CH_4-N_2 collisions, to ensure rotational equilibration for the time × pressure scales used to study vibrational relaxation. The system considered in the kinetic model involves only the 30 vibrational states from the ground state to the tetradecad. Actually, 90 levels have been introduced in the model because of the three nuclear spin modifications existing for methane molecules.

Let us now describe the collisional energy transfer processes taken into account in our model. For the sake of clarity, this

description is given in the case of laser excitation into a rovibrational level of A symmetry that corresponds, for example, to excitation into the $2\nu_3(F_2)$ $J = 1$, A_2, 18 level with the R_0 line. The nuclear spin being conserved upon collisions, the vibrational state, and the spin modification will be specified for methane molecules. (For instance, $CH_4(0, A)$ represents a molecule in the ground state with A spin modification.) There are three main types of processes involved in the relaxation.

1. Intermode Energy Transfer Processes. These processes spread the vibrational energy within a polyad. Such processes can occur upon self-collisions as well as CH_4-N_2 collisions, so in the following processes, M will represent either a methane molecule or a nitrogen molecule. Three types are to be considered:

(a) Transfer between stretching modes $\nu_3 \leftrightarrow \nu_1$:

$$CH_4(\nu_3, A) + M \leftrightarrow CH_4(\nu_1, A) + M \quad (1)$$

Obviously, such processes also occur in the octad; they can be written as

$$CH_4(\nu_3 + \nu_b, A) + M \leftrightarrow CH_4(\nu_1 + \nu_b, A) + M \quad (2)$$

with ν_b corresponding to bending mode ν_2 or ν_4 (two processes), and in the tetradecad for the states containing at least one ν_3 quantum,

$$CH_4(\nu_3 + 2\nu_b, A) + M \leftrightarrow CH_4(\nu_1 + 2\nu_b, A) + M \quad (3)$$

$$CH_4(\nu_3 + \nu_s, A) + M \leftrightarrow CH_4(\nu_1 + \nu_s, A) + M \quad (4)$$

with $2\nu_b$ corresponding to two bending quanta $2\nu_2$, $\nu_2 + \nu_4$ or $2\nu_4$ and ν_s corresponding to one quantum of stretching mode ν_1 or ν_3 (five processes)

(b) Transfer between bending modes $\nu_2 \leftrightarrow \nu_4$:

$$CH_4(\nu_2, A) + M \leftrightarrow CH_4(\nu_4, A) + M \quad (5)$$

In the pentad, there are two processes of this type:

$$CH_4(\nu_2 + \nu_b, A) + M \leftrightarrow CH_4(\nu_4 + \nu_b, A) + M \quad (6)$$

In the octad, there are five processes that may be written

$$CH_4(\nu_2 + \nu_s, A) + M \leftrightarrow CH_4(\nu_4 + \nu_s, A) + M \quad (7)$$

$$CH_4(\nu_2 + 2\nu_b, A) + M \leftrightarrow CH_4(\nu_4 + 2\nu_b, A) + M \quad (8)$$

In the tetradecad, there are eight processes:

$$CH_4(\nu_2 + 3\nu_b, A) + M \leftrightarrow CH_4(\nu_4 + 3\nu_b, A) + M \quad (9)$$

$$CH_4(\nu_2 + \nu_b + \nu_s, A) + M \leftrightarrow CH_4(\nu_4 + \nu_b + \nu_s, A) + M \quad (10)$$

(c) Transfer between stretching and bending modes.

Despite recent progress in spectroscopic studies of the tetradecad,[17,18] the complete analysis in the polyad formalism is not yet available. Predictions of energy levels from the STDS software[19] mention only the main contributing vibrational state with the corresponding wave function mixing ratio. However, predictions of the Dijon group[20] for the energy levels of $2\nu_3(F_2)$ often show a mixing of wave functions between $2\nu_3$ and $(\nu_3 + \nu_2 + \nu_4)$ and also between $(\nu_3 + \nu_2 + \nu_4)$ and $(2\nu_2 + 2\nu_4)$. Although the wave functions of these states are sometimes mixed with other states, we have retained only the $\nu_3 \leftrightarrow (\nu_2 + \nu_4)$ channel for the transfer between stretching and bending modes in order to limit the number of adjustable rate coefficients in the model.

This leads to eight processes in the pentad, the octad, and the tetradecad:

$$CH_4(\nu_3, A) + M \leftrightarrow CH_4(\nu_2 + \nu_4, A) + M \quad (11)$$

$$CH_4(\nu_3 + \nu_b, A) + M \leftrightarrow CH_4(\nu_2 + \nu_4 + \nu_b, A) + M \quad (12)$$

$$CH_4(\nu_3 + \nu_s, A) + M \leftrightarrow CH_4(\nu_2 + \nu_4 + \nu_s, A) + M \quad (13)$$

$$CH_4(\nu_3 + 2\nu_b, A) + M \leftrightarrow CH_4(\nu_2 + \nu_4 + 2\nu_b, A) + M \quad (14)$$

2. Near-Resonant Vibration−Vibration Energy Transfer Processes. These processes involve the exchange of one vibrational quantum between two CH_4 molecules, which occurs only upon self-collisions and distributes the energy among the different polyads. We have taken into account the processes involving the exchange of only one ν_3 or ν_4 quantum.

Because the CH_4 molecules in the ground state may be in any symmetry type A, E, or F, when such a molecule encounters an excited one it can be promoted either to ν_3 or ν_4 according to the process but conserves its symmetry type. Thus, these processes contribute to the distribution of vibrational excitation among the different symmetry species. In the following, we will use S for symmetry species A, E, or F.

(a) Processes involving the exchange of one ν_3 quantum: These are processes of vibrational swap between the ground state and ν_3

$$CH_4(\nu_3, A) + CH_4(0, S) \leftrightarrow CH_4(0, A) + CH_4(\nu_3, S) \quad (15)$$

or more generally

$$CH_4(\nu_3, S) + CH_4(0, S') \leftrightarrow CH_4(0, S) + CH_4(\nu_3, S')$$

Obviously, only processes with $S \neq S'$ are relevant, and processes that couple the tetradecad to the pentad are

$$CH_4(\nu_3 + \nu_s, A) + CH_4(0, S) \leftrightarrow CH_4(\nu_s, A) + CH_4(\nu_3, S) \quad (16)$$

$$CH_4(\nu_3 + 2\nu_b, A) + CH_4(0, S) \leftrightarrow CH_4(2\nu_b, A) + CH_4(\nu_3, S) \quad (17)$$

(b) Processes involving the exchange of one ν_4 quantum.

Processes of vibrational swap between the ground state and ν_4:

$$CH_4(\nu_4, A) + CH_4(0, S) \leftrightarrow CH_4(0, A) + CH_4(\nu_4, S) \quad (18)$$

or

$$CH_4(\nu_4, S) + CH_4(0, S') \leftrightarrow CH_4(0, S) + CH_4(\nu_4, S')$$

Processes coupling the pentad to the dyad + dyad:

$$CH_4(\nu_b + \nu_4, A) + CH_4(0, S) \leftrightarrow CH_4(\nu_b, A) + CH_4(\nu_4, S) \quad (19)$$

Processes coupling the octad to the pentad + dyad, such as

$$CH_4(2\nu_b + \nu_4, A) + CH_4(0, S) \leftrightarrow CH_4(2\nu_b, A) + CH_4(\nu_4, S) \quad (20)$$

or

$$CH_4(\nu_s + \nu_4, A) + CH_4(0, S) \leftrightarrow CH_4(\nu_s, A) + CH_4(\nu_4, S) \quad (21)$$

Processes coupling the tetradecad to the octad + dyad, such as

$$CH_4(3\nu_b + \nu_4, A) + CH_4(0, S) \leftrightarrow CH_4(3\nu_b, A) + CH_4(\nu_4, S) \quad (22)$$

or

$$CH_4(\nu_s + \nu_b + \nu_4, A) + CH_4(0, S) \leftrightarrow CH_4(\nu_s + \nu_b, A) + CH_4(\nu_4, S) \quad (23)$$

A remark must be made at this point about the symmetry of the excited molecules: after excitation into the A symmetry, the only levels in the tetradecad and in the octad that are concerned with the relaxation are of A symmetry. But it is no longer the case for the lower polyads because of the near-resonant V−V transfer processes. Therefore, all the states of E or F symmetry up to the pentad are concerned with the relaxation, and the corresponding intermode and near-resonant V−V energy transfer processes have to be taken into account. Consequently, additional intermode and near-resonant V−V energy transfer processes must be taken into account for the pentad and dyad levels.

3. Vibration to Translation, Rotation (V−T, R) Energy Transfer Processes. The V−T,R processes considered in our model involve the loss of one bending quantum, such as

$$CH_4(\nu_4, S) + M \leftrightarrow CH_4(0, S) + M \quad (24)$$

or

$$CH_4(\nu_2, S) + M \leftrightarrow CH_4(0, S) + M \quad (25)$$

These processes have been taken into account for the ν_2 state and for all levels having at least one ν_4 quantum.

C. Simulation of the Double-Resonance Signals. Finally, from the previous kinetic model, a set of nonlinear differential equations is obtained describing the time evolution of 46 levels (the E or F symmetry levels of the tetradecad or the octad being passive in the case of laser excitation into a $2\nu_3$ A-symmetry level) connected by 99 processes. Laser excitation of methane molecules is modeled by a time-dependent term added to the corresponding differential equation and subtracted from the differential equation of the ground state with A symmetry.

In addition to the processes described so far, diffusion of excited molecules outside the probing beam (or beam fly out) is taken into account by assuming that all excited molecules diffuse out of the probe beam at the same rate δ. This rate is inversely proportional to pressure and can be estimated by[21] $\delta = (^{2.4}/_{R})^2 D$ where D is the diffusion coefficient (in $cm^2\ s^{-1}$) and R the radius of the probe beam (in cm). Diffusion coefficients for self-diffusion as well as diffusion in nitrogen have been calculated from equations and values of Lennard-Jones parameters given in Hirschfelder et al.[22] At 193 K, for 1 Torr of pressure, D is equal to 74.40 $cm^2\ s^{-1}$ for self-diffusion and 74.26 $cm^2\ s^{-1}$ for diffusion in nitrogen. Because these values are very close to each other, the mean value was retained to calculate δ. Hence, at 193 K, δ can vary from 1713 s^{-1} to 10703 s^{-1} for 1 Torr of pressure considering that, under our experimental conditions, the radius of the probe beam R ranges from 0.2 to 0.5 cm. At room temperature, with the same assumptions, δ can vary from 3767 s^{-1} to 23 547 s^{-1} for 1 Torr of pressure.

To limit the number of rate coefficients in the model, some additional assumptions have been made.

1. Simplifying Assumptions. (a) All $\nu_3 \rightarrow \nu_1$ intermode transfer processes considered in the exothermic direction ($\nu_3 > \nu_1$) have the same rate coefficient, $k^{CH4}_{\nu 3 \rightarrow \nu 1}$ for self-collisions and $k^{N2}_{\nu 3 \rightarrow \nu 1}$ for CH_4-N_2 collisions. This rate coefficient is that of the direct exothermic process 1. Similarly, for $\nu_2 \rightarrow \nu_4$ and $\nu_3 \rightarrow \nu_2 + \nu_4$ intermode transfer processes, the rate coefficients $k^{CH4}_{\nu 2 \rightarrow \nu 4}$ (or $k^{N2}_{\nu 2 \rightarrow \nu 4}$) and $k^{CH4}_{\nu 3 \rightarrow \nu 2 + \nu 4}$ (or $k^{N2}_{\nu 3 \rightarrow \nu 2 + \nu 4}$) are those of the direct exothermic processes 5 and 11, respectively.

(b) The rate coefficients of near-resonant V−V transfer processes are related by a scaling factor appropriate to first-order perturbation theory for harmonic oscillators. For instance, the rate coefficient for the process

$$CH_4(2\nu_3) + CH_4(0) \leftrightarrow CH_4(\nu_3) + CH_4(\nu_3)$$

is twice the rate coefficient of process 15, and the rate coefficient of process

$$CH_4(4\nu_4) + CH_4(0) \leftrightarrow CH_4(3\nu_4, A) + CH_4(\nu_4)$$

is 4 times the rate coefficient of process 18. Hence, only two rate coefficients are necessary. The elementary rate coefficients of processes 15 and 18 are noted k_{ν_3} and k_{ν_4} for the exchange of a ν_3 or a ν_4 quantum, respectively.

(c) The rate coefficients of V−T, R transfer processes are related to each other according to the harmonic oscillator approximation; for instance, the rate coefficient of the process

$$CH_4(3\nu_4, S) + M \leftrightarrow CH_4(2\nu_4, S) + M$$

is three times that of process 24. The elementary rate coefficient (i.e., that of process 24) is noted k^{CH4}_{V-T} for self-collisions and k^{N2}_{V-T} for CH_4-N_2 collisions.

All of the rate coefficients for the reverse processes are deduced from the direct ones by applying detailed balance.

2. Resolution of the Set of Differential Equations. These assumptions being made, the number of rate coefficients to be determined is reduced to 10. For given values of the rate coefficients, the time-dependent populations of the 46 levels implied in the overall relaxation process are obtained by solving the set of differential equations with a Runge−Kutta numerical procedure. From the populations of vibrational states, the populations of rovibrational levels have to be deduced in order to simulate double-resonance (DR) signals.

The experimental DR signal is the time-dependent transmitted intensity of the probe beam after laser excitation. Let us consider a probe transition from level v'', J'', S to level v', J', S with the usual notation for vibrational and rotational quantum numbers and S for noting the spin modification (A, E, or F). As long as the variation in intensity is small, the DR signal $I(t)$ can be related to the populations of the upper and lower levels of the probed transition by

$$\frac{I(t) - I_{eq}}{I_{eq}} = G \times \left[\frac{(2J'' + 1)}{(2J' + 1)}(N_{v',J',S}(t) - \bar{N}_{v',J',S}) - (N_{v'',J'',S}(t) - \bar{N}_{v'',J'',S})\right]$$

where G is a factor depending on the transition (wavenumber, Einstein coefficient) and on the absorption length, $N_\alpha(t)$ and $\bar{N}_\alpha$ are respectively the time-dependent population and the

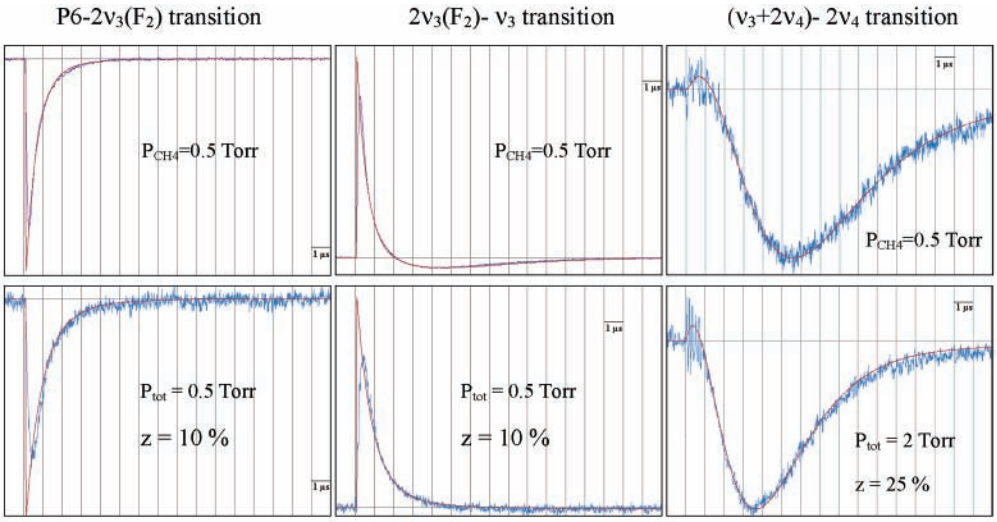

Figure 11. Experimental DR signals and the corresponding simulated DR signals calculated at 193 K using the rate coefficients in Table 1 for various A-symmetry transitions after laser excitation on an A-symmetry level of $2\nu_3(F_2)$.

TABLE 1: Processes and Their Corresponding Rate Coefficients at 193 and 296 K

	193 K		296 K	
processes	rate coefficient in μs^{-1} $Torr^{-1}$	rate coefficient in 10^{-11} cm^3 s^{-1}	rate coefficient in μs^{-1} $Torr^{-1}$	rate coefficient in 10^{-11} cm^3 s^{-1}
$\nu_3 \rightarrow \nu_1$ $k^{CH4}_{\nu3\rightarrow\nu1}$	1.3 ± 0.4	2.6 ± 0.8	1.1 ± 0.3	3.37 ± 0.92
$\nu_3 \rightarrow \nu_1$ $k^{N2}_{\nu3\rightarrow\nu1}$	0.9 ± 0.25	1.8 ± 0.5	0.8 ± 0.3	2.45 ± 0.92
$\nu_2 \rightarrow \nu_4$ $k^{CH4}_{\nu2\rightarrow\nu4}$	2.4 ± 0.4	4.8 ± 0.8	2.2 ± 0.5	6.75 ± 1.53
$\nu_2 \rightarrow \nu_4$ $k^{N2}_{\nu2\rightarrow\nu4}$	>1.4	>2.8	>1.2	>3.68
$\nu_3 \rightarrow \nu_2+\nu_4$ $k^{CH4}_{\nu3\rightarrow\nu2+\nu4}$	1.8 ± 0.2	3.60 ± 0.40	1.5 ± 0.2	4.60 ± 0.61
$\nu_3 \rightarrow \nu_2+\nu_4$ $k^{N2}_{\nu3\rightarrow\nu2+\nu4}$	1.4 ± 0.2	2.8 ± 0.4	1.15 ± 0.15	3.53 ± 0.46
V−V ν_4 mode $k_{\nu4}$	0.58 ± 0.03	1.16 ± 0.06	0.36 ± 0.02	1.10 ± 0.04
V−V ν_3 mode $k_{\nu3}$	0.14 ± 0.04	0.28 ± 0.08	0.08 ± 0.03	0.245 ± 0.092
V−T/R transfer k^{CH4}_{V-T}	$(6.0 \pm 2.0) \times 10^{-4}$	$(1.2 \pm 0.4) \times 10^{-3}$	$(1.05 \pm 0.15) \times 10^{-3}$	$(3.22 \pm 0.46) \times 10^{-3}$
V−T/R transfer k^{N2}_{V-T}	$(6.0 \pm 2.0) \times 10^{-5}$	$(1.2 \pm 0.4) \times 10^{-4}$	$(1.05 \pm 0.15) \times 10^{-4}$	$(3.22 \pm 0.46) \times 10^{-4}$

equilibrium population of level α, and I_{eq} is the transmitted intensity at the Boltzmann equilibrium.

Assuming rotational equilibrium, the time-dependent population of a rovibrational level is simply

$$N_{v',J',S}(t) = \frac{(2J'+1) \times g_S \times \exp(-(E_{v',J',S} - E_{v',S})/kT)}{g_{v'} \times Q_{GS,S}} N_{v',S}(t)$$

where g_S is the spin statistical weight (5, 2, or 3 for S = A, E, or F, respectively), $g_{v'}$ is the vibrational degeneracy, $Q_{GS,S}$ is the rotational partition function in the ground state calculated for levels with spin modification *S*, and $N_{v',S}(t)$ is the time-dependent population of vibrational state v' with spin modification *S* as calculated by the numerical Runge−Kutta procedure described above. Finally, $E_{v',J',S}$ and $E_{v',S}$ are respectively the energies of the v', J', *S* rovibrational level and of the lowest rotational level with spin modification *S* in the vibrational state v'. This description is consistent with the work of Klaassen et al.[5] to model their double-resonance signals after excitation in the octad. These authors have calculated for the A spin modification the rotational partition functions in $\nu_3 + \nu_4$ and in ν_4 and have found a ratio very close to 3, which is the ratio of the vibrational degeneracies. Because we are dealing with the states up to the tetradecad for which the energy levels are not all available, we have assumed, for a given spin modification, that the rotational partition function in a vibrational state v is simply the rotational partition function in the ground state multiplied by the vibrational degeneracy g_v.

The DR signal is then written as

$$\frac{I(t) - I_{eq}}{I_{eq}} = \frac{G(2J''+1)g_S}{Q_{GS,S}} \left[\frac{\exp(-(E_{v',J',S} - E_{v',S})/kT)}{g_{v'}} N_{v',S}(t) - \frac{\exp(-(E_{v'',J'',S} - E_{v'',S})/kT)}{g_{v''}} N_{v'',S}(t) \right]$$

With this procedure, simulated DR signals are calculated for the various probes used in our experiments.

D. Results and Discussion

Rate coefficients for the collisional processes introduced in the kinetic model have been varied until the best agreement was obtained between simulated and experimental signals. This was done for the present experiments at 193 K and also for previous measurements performed at room temperature in methane and in methane−nitrogen mixtures.[1,2] The rate coefficients leading to the best fits at 193 K and at room temperature are reported in Table 1.

Some simulated DR signals obtained using these rate coefficients at 193 K for the probed transitions $3\nu_3-2\nu_3$, $2\nu_3-\nu_3$ and $(\nu_3 + 2\nu_4)-2\nu_4$ are given as examples in Figure 11. They were calculated for pure methane and for mixtures with methane molar fractions of 10 and 25%. They are superimposed on the corresponding experimental signals.

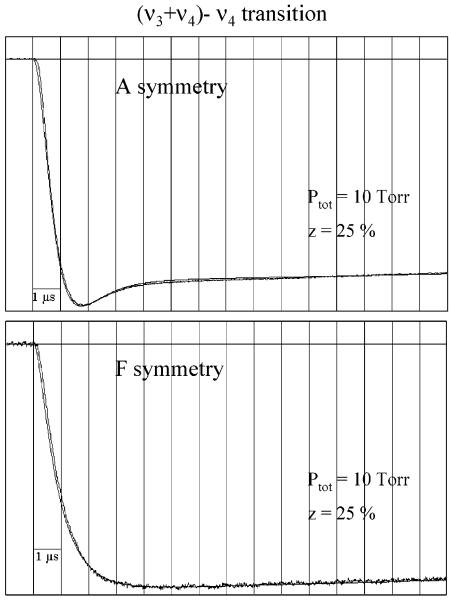

Figure 12. DR signals calculated at 193 K using the rate coefficients of Table 1 for laser excitation on an A-symmetry level of $2\nu_3(F_2)$ and superimposed on the experimental signals.

It can be seen that the agreement is fair in pure methane as well as in methane−nitrogen mixtures with different methane molar fractions, showing that our kinetic model is able to reproduce the temporal evolution of the populations of the tetradecad $2\nu_3$ state and of the pentad ν_3 and $2\nu_4$ states.

Figure 12 presents simulated signals for $(\nu_3 + \nu_4)-\nu_4$ probed transitions in a mixture with a molar fraction of 25% that is also superimposed on experimental signals. Signals of Figure 12 corresponding to probed transitions involving two different symmetry species after laser excitation upon an A-symmetry tetradecad level show that the effect of the pump−probe symmetry type is also well reproduced by the kinetic model. Hence, the hypothesis that the processes implied in the redistribution over the different symmetry species are simply V−V transfer is justified and leads to a good prediction of the redistribution of vibrational excitation among the different symmetry species in the dyad.

The kinetic model has also been tested at room temperature by comparing simulated signals to experimental signals obtained in our previous work.[1,2] Some simulated DR signals obtained using the rate coefficients of Table 1 at room temperature for various probed transitions and methane molar fractions are shown in Figure 13. As for the measurements at 193 K, the agreement is good for all types of probed transition in neat methane as well as in methane−nitrogen mixtures.

Besides the search of the best fit, simulations were carried out to determine the respective influences of the different energy transfer processes on the various types of observed double-resonance signals and to estimate the relative uncertainties of the corresponding rate coefficients. As can be seen in Table 1, all rate coefficients are not determined with the same accuracy. Let us examine how the simulations lead to the uncertainties reported in Table 1.

(a) V−V ν_4 Energy Transfer. The shape of the signals simulated for octad−dyad probe transitions in $CH_4 + N_2$ mixtures with small methane molar fraction, in particular the position of the maximum of absorption of the signal (maximum of population in ν_4), was found to depend strongly on the process of V−V energy transfer in the ν_4 mode. This is illustrated by Figure 14 , where computed DR signals have been plotted for a F-symmetry $(\nu_3 + \nu_4)-\nu_4$ probe transition after an A-symmetry-type excitation at 20 Torr of pressure of a $CH_4 + N_2$ mixture with $z = 0.05$ at 193 K. Signal 1 is obtained using the

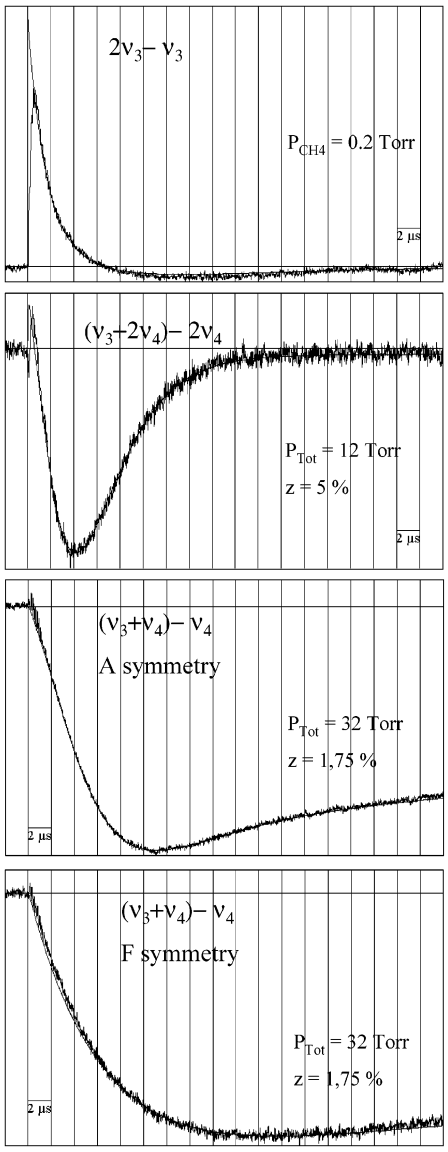

Figure 13. DR signals calculated at 296 K for laser excitation on an A-symmetry $2\nu_3(F_2)$ level and compared to experimental signals.

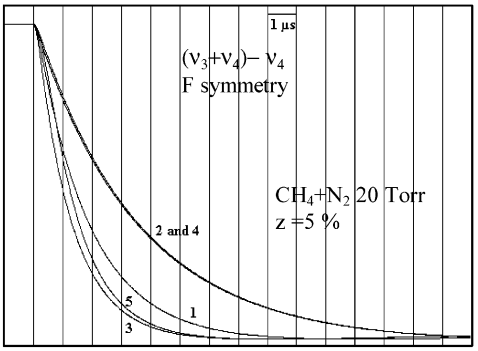

Figure 14. DR signals computed for different values of rate coefficients, assuming laser excitation of A-symmetry species CH_4 molecules. Signal 1: values in Table 1; signals 2 and 3: same as for signal 1 except for the rate coefficient k_{ν_4} taken respectively at 2.9 and 8.7 10^5 s^{-1} $Torr^{-1}$; signal 4: same as for signal 2 but with the rate coefficient of the intermode process $k^{N2}_{\nu3\rightarrow\nu2+\nu4}$ multiplied by 5; signal 5: same as for signal 3 but with $k^{N2}_{\nu3\rightarrow\nu2+\nu4}$ divided by 5.

values of Table 1 whereas for signals 2 and 3 the value of k_{ν_4} has been changed to 2.9×10^5 s^{-1} $Torr^{-1}$ and 8.7×10^5 s^{-1} $Torr^{-1}$, respectively. For such rather small variations (±50%) of k_{ν_4}, the shape of the signal changes rapidly. Keeping the low value of k_{ν_4} as in signal 2 and multiplying by 5 the value of the rate coefficient $k^{N2}_{\nu3\rightarrow\nu2+\nu4}$ does not lead to a recovery of the shape of signal 1, as shown by signal 4 that is almost identical to signal 2. Similarly, signal 5, obtained like signal 3 (high value of k_{ν_4}) but dividing $k^{N2}_{\nu3\rightarrow\nu2+\nu4}$ by 5, is rather close to signal 3, except at the beginning of the decay, the decrease in $k^{N2}_{\nu3\rightarrow\nu2+\nu4}$ causes a kind of delay in the filling of the combination and bending states of the tetradecad. Similar behavior was observed for the maximum of absorption of the signals simulated for the probes $\nu_3 + 2\nu_4 - 2\nu_4$ with a small CH_4 molar fraction ($1\% < z < 10\%$). The same observations apply at room temperature. Because the values giving the best agreement for these two types of signals are consistent, we could obtain k_{ν_4} with a precision of about 5% at 193 K as well as 296 K. It is the most accurate rate coefficient in our model.

(b) V−V ν_3 Energy Transfer. This process has relatively little influence on the DR signals, except for signals obtained in pure methane by probing $2\nu_3-\nu_3$ transitions. This process is mainly effective in the absorbed period of these signals, but $\Delta v_3 = \pm 1$ exchanges are also mixed with the $2\nu_3 \rightarrow \nu_3 + \nu_2 + \nu_4$ and $2\nu_3 \rightarrow \nu_3 + \nu_1$ intermode transfer processes. One could assume that the V−V ν_3 rate constant is equal to zero and that the filling of ν_3 (lower state of the probed transition) is achieved only by a stretching-to-bending transfer in the tetradecad ($2\nu_3 \rightarrow \nu_3 + \nu_2 + \nu_4 \rightarrow 2\nu_2 + 2\nu_4$) followed by V−V ν_4 transfer toward the octad, next the pentad, and finally by a bending-to-stretching transfer in the pentad populating ν_3. This assumption ($k_{\nu_3} = 0$) was tested, but the corresponding computed signals did not reproduce the experimental ones even by taking a very high value for $k^{CH4}_{\nu3\rightarrow\nu2+\nu4}$ (rate coefficient for the $\nu_3 \rightarrow \nu_2 + \nu_4$ transfer).

We concluded that k_{ν_3} has a low but nonzero value determined with an accuracy of 30% due to the interdependence of this constant with others and because only a single type of signal allows us to test its value. Accounting for the error bar of Table 1, the high limit of k_{ν_3} is associated with the low limits for the implied intermode transfer processes.

(c) Intermode Transfer Processes. Among the three types of intermode transfer processes retained in our model, the best determination is obtained for the $\nu_3 \rightarrow \nu_2 + \nu_4$ transfer process that models the stretching-to-bending conversion. This process participates in all of the DR signals obtained in pure methane. The constants that play a major part in the signals of the tetradecad−P6 type are $k^{CH4}_{\nu3\rightarrow\nu2+\nu4}$ (and $k^{N2}_{\nu3\rightarrow\nu2+\nu4}$) and to a lesser extent $k^{CH4}_{\nu3\rightarrow\nu1}$ (and $k^{N2}_{\nu3\rightarrow\nu1}$); this is true in pure methane as well as in mixtures. According to the signals simulated for this type of probe, it arises that $k^{CH4}_{\nu3\rightarrow\nu1}$ and $k^{N2}_{\nu3\rightarrow\nu1}$ must be weaker than $k^{CH4}_{\nu3\rightarrow\nu2+\nu4}$ and $k^{N2}_{\nu3\rightarrow\nu2+\nu4}$, respectively, with a rather broad range of possible values. The comparison with signals observed with probes tuned to $2\nu_3-\nu_3$ does not reduce this range of variation, and the determination of $k^{CH4}_{\nu3\rightarrow\nu1}$ and $k^{N2}_{\nu3\rightarrow\nu1}$ is thus rather unconstrained. The DR signal that is most sensitive to the $\nu_2 \rightarrow \nu_4$ intermode transfer is obtained in pure methane for the $\nu_3 + 2\nu_4 - 2\nu_4$ probes. From this type of signal, $k^{CH4}_{\nu2\rightarrow\nu4}$ is found to be of the same order of magnitude as $k^{CH4}_{\nu3\rightarrow\nu2+\nu4}$ with a correlation between these two constants because it is the combination of both that ensures the filling of $\nu_3 + 2\nu_4$. Hence, when the lowest value is taken for the former, the highest value must be taken for the latter. It is more difficult to obtain $k^{N2}_{\nu2\rightarrow\nu4}$ because, as previously mentioned above, in CH_4-N_2 mixtures simulated $\nu_3 + 2\nu_4 - 2\nu_4$ signals depend especially on V−V energy transfer processes in the ν_4 mode. Consequently, from this type of signal, a minimal value of the rate constant was determined under which the filling of the upper state of the probed transition ($\nu_3 + 2\nu_4$) is not as fast as that observed experimentally. Finally, the upper limit of $k^{N2}_{\nu2\rightarrow\nu4}$ is $k^{CH4}_{\nu2\rightarrow\nu4}$.

(d) V−T Energy Transfer. The rate coefficients of these transfers are 2 or 3 orders of magnitude lower than k_{ν_4} for methane and nitrogen, respectively. These low values make it easy to separate these processes from the other ones and explain the slow increase of the dyad−octad signals. However, this slow increase is also due to the diffusion of the molecules out of the probed volume. The diffusion being inversely proportional to pressure (contrary to any collisional process), the determination of V−T transfer rates should be made from DR signals obtained at high-pressure conditions. But increasing the pressure was hindered by the phenomenon of stimulated emission. In our model, we account for V−T de-excitation processes starting from all of the excited levels having at least one quantum of excitation in ν_4. Because de-excitation upon CH_4-N_2 collision by V−T processes is very slow, V−V processes really play a leading part in the depletion of $2\nu_4$ levels and in the filling of ν_4 levels even for very small methane molar fractions. At 193 K, a molar fraction of approximately 10^{-4} is sufficient for V−T transfers to become as effective as V−V ν_4 transfers. This has implications for the atmosphere of Titan, an atmosphere of nitrogen with a methane concentration of about 10^{-2}. In that case, V−V ν_4 transfers dominate in the de-excitation of methane. If the temperature of the relevant part of the atmosphere of Titan is lower, then this reasoning will still hold because the rate constants of V−T transfers should decrease and those of V−V transfers should increase.

A comparison with existing results can be made for all of the rate coefficients at room temperature[5,23−27] but only for the rate coefficients of V−T de-excitation processes at 193 K.[25−26]

The rate coefficient of V−V ν_4 energy transfer found here, (0.36 ± 0.02) $\mu s^{-1}Torr^{-1}$, is in good agreement with that of Hess et al.,[23] (0.3 ± 0.1) $\mu s^{-1}Torr^{-1}$, and also with that of Klaassen et al.,[5] who give (0.35 ± 0.05) $\mu s^{-1}Torr^{-1}$ for the process of vibrational swap corresponding to our elementary process (eq 18).

For the rate coefficient of V−V ν_3 energy transfer, we obtain a value consistent with that of Hess et al.,[23] (0.125 ± 0.075) $\mu s^{-1}Torr^{-1}$, whereas Klaassen et al.[5] neglect this transfer process. Because the rate coefficient k_{ν_3} is approximately 4 times smaller than k_{ν_4}, when methane molecules are excited on the octad (as in the experiments carried out by Klaassen et al.[5]), the V−V ν_3 transfer process seems to play a minor role in the depletion of the octad.

Both V−V energy transfer rate coefficients increase with decreasing temperature, and this is true whether these rates are given per unit pressure or per unit concentration.

For V−T transfer processes at room temperature, our results are higher but in fair agreement with the results of refs 24−27 for CH_4-CH_4 collisions (giving a rate coefficient in the range of 700−900 s^{-1} $Torr^{-1}$) and with the results of refs 24 and 25 for CH_4-N_2 collisions (60−90 s^{-1} $Torr^{-1}$). At 193 K, this is also the case for self-de-excitation, with the results of refs 25 and 26 lying between 400 and 500 s^{-1} $Torr^{-1}$. Our result at 193 K for CH_4-N_2 collisions presents a larger discrepancy with the only available value[25] of (25 ± 4) s^{-1} $Torr^{-1}$. We notice that for such a small rate coefficient the determination is difficult and the accuracy worsens owing to beam fly out. The temper-

ature dependence of V−T transfer processes is opposite to that of V−V transfer.

With regard to intermode transfers, Hess et al.[23] indicate that the fastest intermode process is the $\nu_3 \rightarrow \nu_1$ transfer at $(1.2 \pm 0.3)\mu s^{-1}$ Torr^{-1} rather than the $\nu_2 \rightarrow \nu_4$ transfer at (1 ± 0.5) μs^{-1} Torr^{-1}. For the rate constant of the stretching-to-bending transfer, assuming the harmonic approximation, they estimate values of 0.3 μs^{-1} Torr^{-1} for the $\nu_3 \rightarrow 2\nu_b$ transfer and 0.6 μs^{-1} Torr^{-1} for the $2\nu_3 \rightarrow \nu_3 + 2\nu_b$ transfer. We are in approximate agreement with these values despite the difference between the constants of the stretching-to-bending transfer and the $\nu_2 \rightarrow \nu_4$ transfer. It is indeed reasonable to obtain larger values when the number of channels for energy transfer is limited. It is more difficult to compare with Klaassen et al.[5] Indeed, these authors consider a "global" model where equilibrium inside the polyads is ensured except for the $(\nu_1 + \nu_4)$ and $(\nu_3 + \nu_4)$ states of the octad (directly concerned with the laser excitation). The value they obtained for the transfer from $(\nu_1 + \nu_4)$ to $(\nu_3 + \nu_4)$ is (0.4 ± 0.1) μs^{-1} Torr^{-1}, which is lower than ours. Finally, the temperature dependence of all intermode transfer processes shows an increase with decreasing temperature when the rate coefficients are given per unit pressure but a decrease when these rates are given per unit concentration. Hence, the probability of transfer for one collision is likely to remain approximately constant from room temperature down to 193 K.

In conclusion, one should never consider the values of the rate coefficients independently from the kinetic model used to derive them. Even if the hypothesis of stretching-to-bending conversion through only one channel may appear to be not very realistic, our model reproduces all of the experimental features well. The current modeling of intermode processes could progress if spectroscopic analyses clarify the "points of passage" for the stretching-to-bending conversion (i.e., the main interactions within the tetradecad). Spectroscopic improvements are also needed for the assignment of new probe lines in hot combination bands such as $(\nu_1 + \nu_3)-\nu_1$, $(\nu_3 + 2\nu_2)-2\nu_2$, or $(\nu_3 + \nu_2 + \nu_4)-(\nu_2 + \nu_4)$. With such probes, processes such as $\nu_2 \rightarrow \nu_4$ and $\nu_3 \rightarrow \nu_1$ transfer could be further investigated.

V. Summary of Conclusions

Rotational depopulation rates were measured at 193 K for self and N_2 collisions with values of (28.3 ± 3.0) μs^{-1} Torr^{-1} and (21.5 ± 3.0) μs^{-1} Torr^{-1}, respectively. These results are in good agreement with line-broadening studies.

Vibrational relaxation was investigated by looking at the time evolution of many states from the dyad to $2\nu_3$ using well-identified DR signals. Kinetic modeling has allowed us to reproduce rather precisely the experimental DR signals at 193 K as well as at room temperature and to obtain rate coefficients of energy transfer processes considered. Further improvements in the modeling of relaxation pathways are dependent on improved spectroscopic analyses of the tetradecad and on reliable assignments of tetradecad−pentad bands.

Acknowledgment. We thank Dr. Claude Camy-Peyret for helpful discussions and for his careful reading of the manuscript.

References and Notes

(1) Menard-Bourcin, F.; Doyennette, L.; Menard, J.; Boursier, C. *J. Phys. Chem. A* **2000**, *104*, 5444.
(2) Menard-Bourcin, F.; Boursier, C.; Doyennette, L.; Menard, J. *J. Phys. Chem. A* **2001**, *105*, 11446.
(3) Yelle, R. V. *Astrophys. J.* **1991**, *383*, 380.
(4) Sang Joon Kim; Geballe, T. R.; Noll, K. S. *Icarus* **2000**, *147*, 588.
(5) Klaassen, J. J.; Coy, S. L.; Steinfeld, J. I.; Abel, B. *J. Chem. Phys.* **1994**, *101*, 10553.
(6) Hepp, M.; Winnewisser, G.; Yamada, K. M. T. *J. Mol. Spectrosc.* **1991**, *146*, 181.
(7) Menard-Bourcin, F.; Doyennette, L. *J. Chem. Phys.* **1988**, *88*, 5506.
(8) The assigned quantum numbers *J*, *C*, and *N* represent the angular momentum, the rovibrational symmetry, and a running number according to increasing energies within the polyads. See Champion, J.-P.; Loëte, M.; Pierre, G. In *Spectroscopy of the Earth's Atmosphere and Interstellar Medium*; Rao, K. N., Weber, A., Eds.; Academic Press: Boston, 1992; pp 339−422.
(9) Kalinin, D. V.; Bronnikov, D. K.; Selivanov, Y. G.; Gabard, T.; Champion, J.-P.; Hilico, J.-C. *J. Quant. Spectrosc. Radiat. Transfer* **1999**, *62*, 13.
(10) Pine, A. S. *J. Chem. Phys.* **1992**, *97*, 773 and references therein.
(11) Pine, A. S. *J. Quant. Spectrosc. Radiat. Transfer* **1997**, *57*, 157.
(12) Benner, D. C.; Malathy Devi, V.; Smith, M. A. H.; Rinsland, C. P. *J. Quant. Spectrosc. Radiat. Transfer* **1993**, *50*, 65.
(13) Smith, M. A. H.; Rinsland, C. P.; Malathy Devi, V.; Benner, D. C. *Spectrochim. Acta, Part A* **1992**, *48*, 1257.
(14) Boussin, C; Regalia, L.; Plateaux, J.-J.; Barbe, A. *J. Mol. Spectrosc.* **1998**, *191*, 381.
(15) Singh, K; O'Brien, J. J. *J. Quant. Spectrosc. Radiat. Transfer* **1994**, *52*, 75.
(16) Varanasi, P.; Chudamani, S. *J. Quant. Spectrosc. Radiat. Transfer* **1989**, *41*, 335.
(17) Robert, O.; Hilico, J.-C.; Loëte, M.; Champion, J.-P.; Brown, L. R. *J. Mol. Spectrosc.* **2001**, *209*, 14.
(18) Georges, R.; Herman, M.; Hilico, J.-C.; Robert, O. *J. Mol. Spectrosc.* **1998**, *187*, 13.
(19) Wenger, C.; Champion, J.-P. *J. Quant. Spectrosc. Radiat. Transfer* **1998**, *59*, 471 (Spherical Top Data Systems (STDS) software for the simulation of spherical top spectra).
(20) Robert, O.; Champion, J.-P. Private communication.
(21) Margottin-Maclou, M.; Doyennette, L.; Henry, L. *Appl. Opt.* **1971**, *10*, 1768.
(22) Hirschfelder, J. O.; Curtiss, C. F.; Bird, R. B. *Molecular Theory of Gases and Liquids*; Wiley: New York, 1964.
(23) Hess, P.; Kung, A. H.; Moore, C. B. *J. Chem. Phys.* **1980**, *72*, 5525.
(24) Yardley, J. T.; Fertig, M. N.; Moore, C. B. *J. Chem. Phys.* **1970**, *52*, 1450.
(25) Siddles, R. M.; Wilson, G. H.; Simpson, C. J. S. M. *Chem. Phys.* **1994**, *188*, 99.
(26) Perrin, M.-Y.; Jolicard, G. *Chem. Phys. Lett.* **1986**, *127*, 118.
(27) Avramides, E.; Hunter, T. F. *Chem. Phys.* **1988**, *88*, 5506.